FINAL REPORT

Validation Study of Wave Breaking Influence in a Coupled Wind Wave Model for Hurricane Wind Conditions

Michael L. Banner
School of Mathematics, The University of New South Wales, Sydney 2052, Australia
Tel: (+61-2) 9385-7072 fax: (+61-2) 9385-7123 email: m.banner@unsw.edu.au

Russel P. Morison
School of Mathematics, The University of New South Wales, Sydney 2052, Australia
Tel: (+61-2) 9385-7080 fax: (+61-2) 9385-7123 email: r.morison@unsw.edu.au

Lance M. Leslie
School of Meteorology, The University of Oklahoma, Norman, OK 73019, USA
Tel: (405) 325-0596; fax: (405) 325-7689; email: lmleslie@ou.edu

Award No. N0001-00-1-0288

Submission Date: 27 August, 2008

REPORT DOCUMENTATION PAGE

Form Approved
OMB No. 0704-0188

1. REPORT DATE *(DD-MM-YYYY)*	2. REPORT TYPE	3. DATES COVERED *(From - To)*
31-08-2008	Final report	1 January, 2000-31 May, 2008

4. TITLE AND SUBTITLE
Validation Study of Wave Breaking Influence in a Coupled Wind Wave Model for Hurricane Wind Conditions

5a. CONTRACT NUMBER

5b. GRANT NUMBER
N00014-00-1-0288

5c. PROGRAM ELEMENT NUMBER

6. AUTHOR(S)
Banner, Michael L.; Morison, Russel P.; Leslie, Lance M.

5d. PROJECT NUMBER

5e. TASK NUMBER

5f. WORK UNIT NUMBER

7. PERFORMING ORGANIZATION NAME(S) AND ADDRESS(ES)
School of Mathematics and Statistics, The University of New South Wales, Sydney 2052, Australia

8. PERFORMING ORGANIZATION REPORT NUMBER
None

9. SPONSORING/MONITORING AGENCY NAME(S) AND ADDRESS(ES)
Grant Management Organisation, The University of New South Wales, Sydney 2052, Australia

10. SPONSOR/MONITOR'S ACRONYM(S)
GMO

11. SPONSOR/MONITOR'S REPORT NUMBER(S)
None

12. DISTRIBUTION/AVAILABILITY STATEMENT
Unlimited

13. SUPPLEMENTARY NOTES

14. ABSTRACT
As marine winds strengthen, wave breaking becomes increasingly widespread with potentially important consequences for offshore operations. Wave breaking is not included in present marine forecasts. This project addressed the incorporation of wave breaking physics into coupled sea state marine weather forecasting models, with aim of adding accurate wave breaking forecasts to the standard sea state variables. Our approach combined observational and modeling efforts. New results from our field data analyses were synthesized into accurate parameterizations for wave breaking occurrence and strength. The wind input source term was modified for compatibility with the other source terms and physical constraints. These refinements were incorporated in the dissipation and wind input source terms in the spectral wave evolution models used to generate forecasts. The model output results were evaluated critically in systematic tests from moderate to severe wind speeds. After extensive iterations, the model framework is ready for implementation and further testing in operational prototype models.

15. SUBJECT TERMS
Wind wave modeling, sea state forecasting, wave breaking

16. SECURITY CLASSIFICATION OF:			17. LIMITATION OF ABSTRACT	18. NUMBER OF PAGES	19a. NAME OF RESPONSIBLE PERSON
a. REPORT	b. ABSTRACT	c. THIS PAGE			Dr. Michael L. Banner
U	U	U	UU	33	19b. TELEPHONE NUMBER *(Include area code)* +612-9958-5136

Executive Summary

As marine winds strengthen, wave breaking becomes increasingly widespread. This has important consequences, both for offshore operations and geophysically, yet wave breaking is not included in present marine forecasts. This project addressed the incorporation of wave breaking physics into coupled sea state marine weather forecasting models. The aim was to add accurate wave breaking forecasts to the standard sea state variables, with the model validity spanning light to very severe sea state conditions.

Our approach required a combination of observational and modeling efforts. We synthesized results from our field data analyses into accurate parameterizations for wave breaking occurrence and strength. We also needed to modify the wind input source term for compatibility with the other source terms and physical constraints. These refinements were incorporated in the dissipation and wind input source terms in the spectral wave evolution models used to generate forecasts.

Model development focused on wide spectral bandwidth computations of the directional wave spectrum and its tail region. We used an 'exact' version of the nonlinear wave-wave interaction source term in the radiative transfer equation for the wave field. We carefully validated cases for which data exists, ensuring that the modeled wave properties, wind input and upper ocean dissipation rates are all consistent with observed levels. This was a key focus of our effort since matching the source term levels over a wide range of wind speeds is essential for reliable forecasts of breaking waves and the enhanced air-sea fluxes they generate.

The model output results were evaluated critically in systematic tests from moderate to severe wind speeds. After extensive iterations, the model framework is ready for implementation and further testing in operational models. Given that our framework used the 'exact' form of the nonlinear wave-wave interaction, we anticipate that the least amount of adaptation and best results will be obtained if the new TSA (Two Scale Approximation) source term for the nonlinear interactions (Resio and Perrie, 2008) is used, replacing the standard DIA source term.

An auxiliary effort was conducted within this project that investigated parameterizing sea spray flux in terms of breaking wave properties rather than wind speed. A laboratory study (SPANDEX) was undertaken to refine sea spray flux dependences in severe conditions, and a sea state dependent spray source function was formulated.

Overall, when this project commenced in FY00, existing knowledge on wave breaking was scant, and it was necessary to advance knowledge of the fundamental physics of wave breaking in order to be able to incorporate this process reliably into forecast models. Very significant progress on the scientific fundamentals was achieved in this project in parallel with our modeling effort. The modeling framework that has been developed for forecasting the breaking properties of the dominant waves is ready for operational implementation. The physics of short breaking waves still remains elusive and accurate modeling of these scales is not yet feasible. Nonetheless, the capacity to include dominant wave breaking properties as part of operational sea state forecasts will increase both the accuracy and utility of the next generation of operational coupled sea state and ocean weather forecasting models, particularly in severe to extreme sea states.

TABLE OF CONTENTS

1. BACKGROUND / PROBLEM STATEMENT

1.1 Wave breaking in coupled air-sea interaction modeling

Under strong forcing conditions, breaking waves are a conspicuous feature of the wind-driven sea surface, appearing as whitecaps. The impact forcing of large breaking waves provides the greatest safety challenge to shipping and coastal structures. Their overturning of the air-sea interface profoundly influences the dynamics and thermodynamics of the boundary layers of the upper ocean and the marine atmosphere. Consequences of breaking in the upper ocean surface layer include greatly enhanced observed turbulence dissipation rates in the near-surface region (e.g. Terray et al., 1996, Gemmrich and Farmer, 2004). In the atmospheric marine boundary layer, increased wave form drag results from the separated air flow over breaking waves. This is accompanied by augmented sea spray, bubbles and acoustic underwater noise, as well as enhanced microwave backscatter and emissivity. These numerous and diverse aspects of wave breaking, described in greater detail in review articles (e.g. Banner and Peregrine, 1993, Thorpe, 1993 and Melville, 1996).

Given the important role of wave breaking in air-sea fluxes, we set out to include this widespread process more explicitly in the next generation of fully-coupled forecast models for the atmosphere-ocean system. The aim of this project was to conduct the research needed to address this challenge, as no such modeling capability presently exists. Forecasts of breaking wave properties provide practical wave climate information for sea keeping. The approach pursued was to develop more realistic parameterizations for wave breaking occurrence and strength, and to validate them against observations in test-bed models. The end goal was to be able to refine these improvements ready for use in an operational marine forecast system, such as the COAMPS/WaveWatch III model. There are also enhanced scalar air-sea fluxes associated with wave breaking, including sea spray, bubbles and greenhouse gases. Such information is needed to underpin future operational versions of coupled atmosphere-wave-ocean models.

1.2 Wind wave modeling

In present wind wave forecast models, breaking waves only appear implicitly as part of the spectral dissipation source term. Otherwise, they receive no direct quantification. These models compute the evolution of the directional wave height spectrum $F(k,\theta; x,y,t)$ under the resultant of the spectral source terms, according to the radiative transfer equation (assuming deep water and no currents):

$$\frac{\partial F}{\partial t} + \vec{c}_g \cdot \nabla F = S_{tot} \qquad (1)$$

where $F = F(k,\theta)$ is the directional wave spectrum, $\vec{c}_g$ is the group velocity. The total source term $S_{tot} = S_{in} + S_{nl} + S_{ds}$, where S_{in} is the atmospheric input spectral source term, S_{nl} is the nonlinear spectral transfer source term representing nonlinear wave-wave interactions and S_{ds} is the spectral dissipation rate, primarily due to wave breaking.

The wind input term is synthesized from ocean, laboratory measurements and idealized mathematical models. The nonlinear transfer term is derived from weakly nonlinear spectral interactions for an ensemble of irrotational gravity wave Fourier modes (Hasselmann, 1960). The dissipation term was formulated to close the problem and is based on a decay rate formulation controlled by an integral spectral wave steepness parameter.

It should be noted that the source terms presently used in these models are heavily tuned to produce wave height spectral estimates that agree well with corresponding observations. This

does not validate the relative strength of the three source terms, which is more difficult to assess. One option is to compare computed and measured integrated wind input and dissipation rates, for which the integrated nonlinear transfer term vanishes. Unfortunately, neither the integrated wind input or dissipation rate is computed reliably in the models, nor are they easily measured. Hence this approach has not been actively pursued by investigators. However, the recent availability of systematic breaking wave data provides a robust basis for discriminating between alternative wind input and dissipation rate source terms, and was exploited in this project.

1.3 Breaking wave physics and observations

This investigation both motivated and generated several significant advances in breaking wave observations and analysis. Prior to this project, available wave breaking field data showed a very large scatter when plotted against standard sea state variables such as wind speed or wave age (e.g. see Figs. 7 and 8 in Gemmrich and Farmer, 1999).

Shortly before this project commenced, the observational study by Banner et al. (2000) reported a strong correlation of breaking probability of dominant wind waves with their significant steepness above a threshold level. However, the present project needed an extension of this class of result beyond the dominant waves to the shorter waves in the spectrum. The 1999 Pacific Ocean storm waves data set gathered by Gemmrich and Farmer (IOS, Canada) provided this opportunity. Described below are details of this part of the project. The resulting paper (Banner et al., 2002) proposed a common breaking threshold that is applicable across different wave scales. This threshold is based on the wave saturation spectrum, and has contributed key elements of our spectral dissipation rate modeling effort.

To validate our breaking wave forecasts, we needed a spectral measure to quantify wave breaking. This was provided by the spectral density of breaking crest length/unit area ($\Lambda(c)$) introduced by Phillips (1985). Initial measurements of $\Lambda(c)$ are now available through remotely sensed imagery, and have been of primary importance in calibrating the source terms in this study. A detailed description of $\Lambda(c)$ is given in section 2.1.2. While $\Lambda(c)$ is a key validation variable, it is kinematic in nature. A breaking strength parameter is still needed to accompany $\Lambda(c)$, which is also discussed in detail in section 2.1.2.

2. TECHNICAL APPROACH

We developed a modeling framework and performed numerical model calculations for wind wave spectral evolution. The output was validated against a set of benchmarks based on field measurements. The source terms were refined iteratively to improve the model performance. Due to the complex nature of the 'exact' nonlinear wave interaction source term, the calculations typically needed 24-48 hours of CPU time to process the evolution to full development. Also, this project required a strong synergy between our modeling effort and basic knowledge of the physics of breaking, including the analysis of field observations. This was an essential element that underpinned our progress throughout the project.

2.1 Breaking wave observational inputs

Fundamental observational contributions on breaking waves generated within this effort were introduced briefly in section 1.3, and are highlighted in section 3.1. Detailed results are described in sections 4.1 and 4.2.

These results materially advanced the development of our goal of including breaking wave physics in our model framework. Key elements were (i) the formulation and refinement of the spectral dissipation rate source term S_{ds} (ii) the extraction of spectral breaking wave crest length and strength (iii) incorporating the strong enhancement of the local wind momentum flux to the waves over breaking waves into the wind input parameterization term (Banner, 1990).

2.1.1 Breaking onset dependence on spectral saturation

A collaborative study was undertaken with Gemmrich and Farmer at IOS Canada involving a novel scale analysis of breaking waves. This was motivated by the results of the model study of wave breaking onset by Song and Banner (2002), who identified the wave energy convergence rate and geometrical steepening within nonlinear wave groups as key factors in breaking onset. From their study (Banner et al., 2002) showed that a common breaking threshold based on a parametric growth rate for these processes collapsed the breaking probability data over an appreciable range of wave scales.

Motivated by the Song and Banner (2002) nonlinear wave group approach, the directionally-normalized spectral saturation $\tilde{\sigma}(f)$ was chosen as the surrogate for local wave nonlinearity. It is given by

$$\tilde{\sigma}(f) = (2\pi)^4 f^5 F(f)/2g^2/\Theta(f) \qquad (2)$$

where f is the wave frequency, F(f) is the wave energy spectrum and $\Theta(f)$ is the directional spreading width spectrum.

The results, described in detail in section 4.1.1 below, provided direct input into the formulation of the dissipation source term and into our procedure for extracting breaking wave properties. More specifically, the component of our S_{ds} formulation associated with direct breaking at a given scale was built around the observed normalized saturation threshold for the dissipation rate associated with wave breaking. Suitable spectral smoothing was applied in the measurements of (2) reported below.

2.1.2 Spectral density of breaking crest length/unit area and breaking strength parameter

The spectral measure of breaking waves $\Lambda(\mathbf{c})$ has the property that $\Lambda(\mathbf{c})\,d\mathbf{c}$ gives the crest length/unit surface area of breaking crests traveling with velocities in ($\mathbf{c}$, $\mathbf{c}$+d$\mathbf{c}$). In this study,

$\Lambda(\mathbf{c})$ was one of the primary breaking forecast parameter computed in our modeling effort. It was also used to model breaking wave enhancements to the wind stress. The contributions of allied air-sea fluxes such as sea spray based on the sea state rather than on the wind field can also be quantified via $\Lambda(\mathbf{c})$.

A measure of breaking strength is needed to quantify the wave energy loss rate through breaking associated with a given Λ distribution. The connection between these two distributions was assumed to be given by the scalar form of equation (6.3) in Phillips (1985):

$$\varepsilon(c)\, dc = b g^{-1} c^5 \Lambda(c)\, dc \qquad (3)$$

where the non-dimensional coefficient b reflects the breaking strength.

Underlying (3) is the assumption that the mean wave energy dissipation rate at scale (c, c+dc) is associated entirely with wave breaking at that scale. This is likely to be most valid around the spectral peak, and this was confirmed in this study. However, (3) may have shortcomings for calculating Λ levels for shorter breakers due to the attenuation of short wave energy by the passage of longer breaking waves (Banner et al., 1989). Thus a more realistic form for S_{ds} should have a 'local' spectral contribution from the actively breaking short waves plus a background attenuation component representing the cumulative attenuation of short waves by longer breaking waves sweeping through them, in addition to the residual turbulence in the wave boundary layer which is operative in attenuating all wave scales.

We examined various forms for refining (3) to account for these effects. As will be seen below, the data reveals a very strong attenuation of breaking waves for speeds below about $0.2c_p$, where c_p is the speed of the spectral peak waves. Despite considerable effort, we were not able to understand the underlying physics, which makes modeling this effect speculative. Hence we decided to parameterize breaking effects for wave shorter than the spectral peak waves. We focused our attention on forecasting the breaking of the energetic waves at the spectral peak, as these are likely to be the dominant breaking wave scale in growing seas as well as in very severe sea states, where the dominant waves are usually very strongly forced. The methodology we developed is described in section 3.2.1 below.

Even assuming that (3) provides the dominant contribution to S_{ds}, the dependence of breaking strength b on the wave variables is not yet fully understood. The expectation is that b should increase systematically with wave nonlinearity. In a recently published paper linked to this project, Banner and Peirson (2007) found a strong correlation for b with the energy convergence rate within narrow-band nonlinear wave groups. These direct measurements reported b values increasing linearly from 8×10^{-5} to 1.2×10^{-3} as the convergence rate parameter increased. More recently, Tian et al. (2008) have confirmed this trend.

Initial field measurements of $\Lambda(c)$ and b were published in the early years of this project (Phillips et al, 2001, Melville and Matusov, 2002). However, we had concerns about key aspects of the data processing in these studies. Also, these data were taken only during fully developed sea states, while data for growing seas as well as developed wind seas were clearly needed. Such data had been collected from RV FLIP in October 2000 during the ONR FAIRS project (http://airs.apl.washington.edu/projects/fairs/summary.html). A collaboration was initiated with J. Gemmrich and C. Garrett at University of Victoria, BC, Canada, to process this archived data. This has provided a unique set of results for both Λ and the mean breaking strength <b>, highlighted below in section 4.3, that have been a primary validation source for our model

development. The uniqueness of this data set lies in its coverage of a growing wind sea that matures - previous observations have been only of mature sea states.

2.2 Modeling objectives and approach

The overall objective was to develop and refine our model framework to be able reproduce over a wide range of wind speeds the field-observed benchmarks A - E stated below in section 2.2.2. Further, this refined modeling framework should be suitable for transitioning to operational forecasting in the next generation of coupled atmosphere/sea state/upper ocean circulation models.

2.2.1 Approach

Wave model

We developed a model framework with a spectral dissipation source term S_{ds} that embodies the threshold nature of breaking. This term was assumed to depend on wave parameters and emphasizes the saturation threshold behaviour reported by Banner et al. (2002). The approach was based on treating waves in different directional spectral bands as nonlinear wave groups. It belongs to the class of nonlinear forms of S_{ds} discussed by Donelan and Yuan in §II.4 of Komen et al. (1994). This form of S_{ds} provides a method for calculating Λ, the spectral density of breaking crest length/unit area (defined above in section 2.1.2). Details of this form of S_{ds} are given in section 3 below. In addition to the S_{ds} term, we needed a suitable wind input source term, having committed to use the 'exact' form of nonlinear spectral transfer term S_{nl}. Special attention was given to ensuring a close match between the total energy flux to the waves and the total water-side dissipation rate in the wave boundary layer.

Wind forcing model

Our strategy in this project was to utilize an accurate wind input source term to drive the model, with an appropriate level of coupling so that future transition to a fully-coupled atmospheric boundary layer model would be straightforward. This required very considerable effort and proved to be very challenging, given the large dynamic range of growth rates in existing wind input source term formulations. In fact this project became a de facto test-bed for wind input source terms, as our model validation procedure placed the most stringent demands on this source term for compatibility with the other source terms and matching to observations, as outlined in section 2.2.2. Details of our evaluation procedure and the final form of our wind input source term implementation are described in section 3.2.1.

2.2.2 Modeling benchmarks

A. evolution of non-dimensional mean wave energy E and spectral peak frequency f_p

B. spectral tail properties: mean directional spreading with k/k_p; spectral saturation; level and exponent of 1D transect k-spectrum (k is the wavenumber, k_p is the spectral peak wavenumber)

C. validating the relative size of the computed wave-induced stress levels (non-breaking and breaking) relative to overall wind stress driving the model.

D. prediction of breaking crest length/unit area spectral density Λ and breaking strength b of the dominant (spectral peak) wind waves at different wave ages.

E. ensuring the modeled integrated water-side dissipation rates match observed levels, and are consistent with the integrated energy flux from the wind to the waves.

2.2.3 Spectral bandwidth of the calculations

We ran broad spectral bandwidth computations of the evolution of the directional wave spectrum and its tail region using an 'exact' version of the nonlinear wave-wave interaction source term S_{ds} in the radiative transfer equation for the wave field. Our S_{ds} needed to be uncompromised by approximations in S_{nl}. We used the 'exact' form of S_{nl} to avoid the known errors associated with 'discrete interaction approximation' implementations in use operationally.

The consequence of using an 'exact' form of S_{nl} was very long computational times throughout the whole project, due to the millions of interactions that need to be calculated at each space or time step in the evolution. This effect becomes more pronounced at higher wind speeds, where the time or space step needed to be shortened for stability. At hurricane wind speeds, model runs to well-developed seas required several days to finish. Before proceeding with the calculations, we invested very considerable effort in evaluating various versions of the 'exact' S_{nl} code and propagation/stepping schemes available to us. This was to ensure accuracy and minimize computational instabilities that can develop at higher wavenumbers.

For our standard computations, we concentrated on duration-limited growth cases, which were the least prone to spurious numerical instability. There are established non-dimensional duration-limited growth correlations for wave energy and peak frequency based on field observations (Young, 1999). These can also be inferred from fetch-limited observations by the methodology discussed in Hwang and Wang (2004). In our calculations, a variable logarithmic grid was developed and implemented to accommodate the evolution from very young to very old wind seas over the wide range of wind speeds investigated.

3. TECHNICAL ACTIVITIES PERFORMED

3.1 Observational data analysis effort

Brief summaries only are included here as these contributions either appear or will soon appear in the open literature. The key results from these papers are highlighted in section 4.1 for convenient reference in this report.

Banner, Gemmrich and Farmer (2002): demonstrated a strong ordering of breaking probability on a spectral measure (normalized saturation) of wave nonlinearity, and established a robust breaking threshold across a significant spectral range of wave scales.

Banner and Peirson (2007): established the dependence of wave breaking onset and strength for weakly nonlinear wave groups in a detailed laboratory wave tank study. They investigated the breaking prediction performance of the Song & Banner (2002) parametric growth rate parameter that combines wave energy convergence and geometrical steepening. They also established the dependence of the breaking strength parameter 'b' on this growth rate parameter.

Gemmrich, Banner and Garrett (2008): provided the first reliable data set for field observations of $\Lambda(c)$ and b that have accompanying wave height spectra, wind stress, wind speeds and integrated water-side dissipation rate estimates for an evolving open ocean wind sea. Their study provided the central observation validation data for this project.

Fairall, Banner, Asher, Peirson and Morison (2008): is the first study seeking to relate sea spray flux directly to breaking wave surface disturbance properties, rather than wind speed. The novel results revealed a strong threshold behaviour, with a quasi-linear increase in spray flux with breaking energy intensity and near-surface wind speed.

3.2 Model development, computations and refinement

3.2.1 Details of Source Term Development

A. Spectral dissipation rate source term S_{ds}

We refined the saturation threshold form of the dissipation rate source term S_{ds} proposed by Alves and Banner (2003), incorporating the observed breaking saturation threshold reported by Banner et al. (2002) (see Figure 1, section 4 below). Also, various refinements were introduced to shape its spectral distribution, in order to provide a much better match to the wind input source function S_{in} at higher wavenumbers, and to our recently published observations of the spectral density of breaking wave crest length/unit area (Gemmrich et al., 2008).

In the present study, S_{ds} was composed of a local breaking term S_{ds}^{loc} plus a parametric background dissipation rate due to background turbulence and the effect of longer breaking waves attenuating shorter waves.

The form of S_{ds} used in this study is shown in (4) below. It uses a power law function of the normalized spectral saturation ratio to reflect the observed breaking threshold behaviour, and refines the form proposed by Alves & Banner (2003). The form used here is

$$S_{ds}(\mathbf{k},\theta) = C[(\tilde{\sigma} - \tilde{\sigma}_T)/\tilde{\sigma}_T)^a + \varepsilon_{res}](\sigma/\sigma_m)^b \, \omega \, F(\mathbf{k},\theta) \qquad (4)$$

In (4), σ and $\tilde{\sigma}$ are the saturation and saturation normalized by the mean directional spreading width, $\tilde{\sigma}_T$ is threshold normalized saturation and σ_m is the saturation at k_m, the mean wavenumber at the transition from the peak enhancement region to the spectral tail. The breaking threshold switching exponent *a* was taken as 2, and *b* was taken as 4, based on matching to the high wavenumber forms of $S_{in}(k)$. The coefficient C was chosen to provide the optimal match to observed duration evolution data of the spectral peak energy and peak frequency (e.g. Young, 1999). It is evident that C needs to increase with the wind speed, since the integrated dissipation rate must balance the integrated wind input for developed seas. It is possible to have C depend on a wave field parameter that is wind speed dependent, such as the mean square slope [mss], and we proceeded on this basis.

The term ε_{res} in (4) is a nonlocal background dissipation coefficient and its form is not known. We assumed that it scales with the mean steepness parameter Ek_p^2, where E is the total wave energy and k_p is the spectral peak wavenumber. An associated proportionality constant of 0.125 was determined through model runs over the wind speed range 5-60 m/s, for which its performance was found to be effective. While not addressed directly in this study, it is straightforward to extend this parameterization to provide attenuation rates consistent with observed decay rates of swell leaving storm areas.

The proposed form (4) of S_{ds} refines the integral wave steepness threshold used in the quasilinear form of S_{ds} presently used in most operational sea state forecast models.

As the project progressed, we were able to significantly refine our capability for calculating the spectral density of mean breaking wave crest length/unit area for the *dominant* wind seas to the point where we achieved close agreement with the observed levels for both developing and mature seas for the only such data set available (Gemmrich et al., 2008).

However, for the short breaking waves in the spectral tail, there remains a substantial unresolved difference between the model predictions and the observations. We investigated a range of possible refinements to the spectral distributions of the wind input and dissipation rates to the short gravity wave scales in order to provide a better match to the observations, but reconciling the short wave breaking properties provided a very substantial challenge which was not resolved in this project. This is discussed further in section 4.2.1 under 'Breaking wave forecasts'.

B. Spectral nonlinear transfer rate source term S_{nl}

The version of 'exact' S_{nl} used was a recent update (Don Resio, private communication) of Tracy and Resio (1982) with $\pm 180^\circ$ directional coverage. Our decision to run a wide spectral bandwidth required careful testing for high wavenumber instabilities and was expensive in both development and computational time. The instabilities were minimized by using short timesteps, a low level of source term filtering and initial dampening of rates of change. Also, energy removal at high wavenumber end of the grid achieved by imposing a k^{-4} tail termination on the computed solution, thereby suppressing any accumulation at the end of grid associated with S_{nl}. The model output verified that the nonlinear transfer term had zero net integral at all times.

C. Spectral wind input source term S_{in}

We sought a form of the wind input source term S_{in} with a plausible distribution of wind input to both fast and slower moving waves that provides accurate energy input levels from weak to hurricane forcing conditions, consistent with observational data. As our effort progressed, we discovered that most of the proposed forms for S_{in} are non-optimal in this respect if reliable

forecasts are sought for wave breaking properties.

The magnitude and spectral composition of the wind input source term S_{in} are imprecisely known, despite very considerable observational and theoretical study over the past few decades. We investigated a number of proposed S_{in} formulations. Among the forms of S_{in} selected for testing were (i) Hsiao & Shemdin (1983) and (ii) Janssen (1991). We also investigated a form based on the wind strength forcing a spectral component at a height of half of its wavelength. The latter departs appreciably from the usual formulation based on the friction velocity u_* or a fixed wind speed, such as U_{10}. This form was proposed in the Lake George shallow water wave study (Donelan et al., 2006), but it was found to be far too strong in our application. We note that (i) is based on a set of field observations using a wave-follower while (ii) is based on the critical layer theory of Miles (1957) and is tuned closely to available field measurements of Snyder et al.(1981) and laboratory measurements (Plant, 1982). The differences between forms (i) and (ii) are indicative of the level of uncertainty between the S_{in} forms used in different contemporary wave models. Figure 1 below shows their non-dimensional growth rates for developing and mature wind seas. Note that they differ very considerably in regard to their spectral levels for weakly and strongly forced scales.

Following detailed testing, we found that the spectral distribution of the growth rate was crucial to the successful modeling of the breaking properties of the spectral peak waves. With too low a level of input to the dominant waves, there was insufficient excess energy flux to these waves to account for the observed breaking levels. This key factor limited out attention to the Janssen (1991) form for S_{in}, which was modified as discussed in the following section.

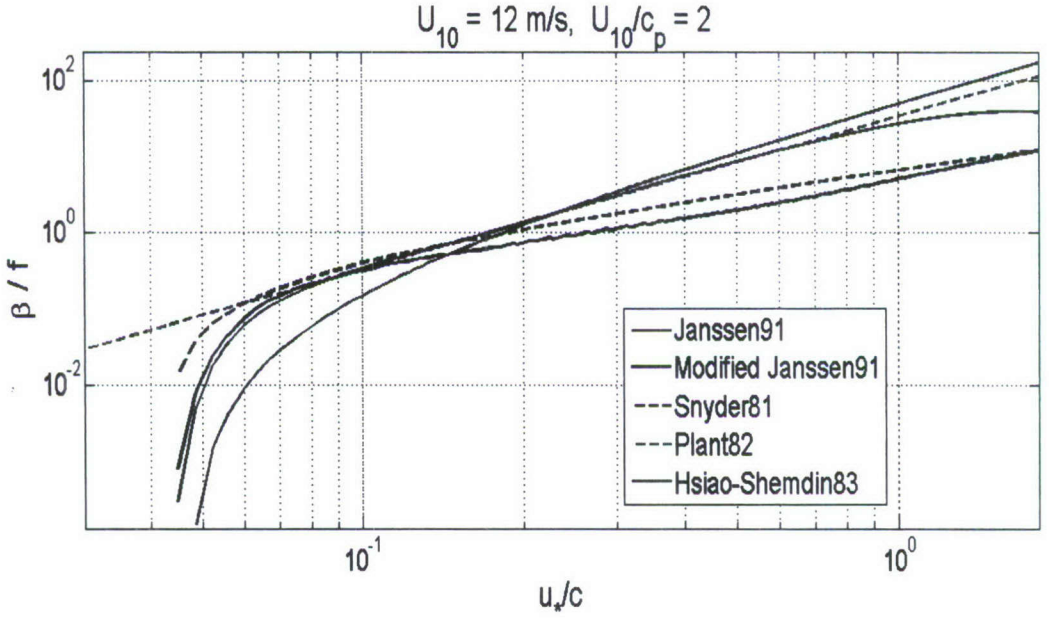

Figure 1. Plot showing the considerable differences between the spectral growth rate β of selected data set parameterizations (Snyder, 1981; Plant, 1982; Hsaio-Shemdin, 1983) for growing seas (U_{10}/c_p~2). The Janssen91 parameterization is consistent with Snyder81 for fast (longer) waves and Plant82 for the slow (short) waves. The difference between the Janssen91 and modified Janssen91 curves shows the extent of sheltering introduced for the shorter waves. This was found to be sufficient to align the computed wind stress with observed levels.

Sheltering

We made an essential modification to the Janssen (1991) input source term in the spirit of the notion of 'sheltering' (e.g. Makin & Kudryavtsev, 2001), amongst others. Conceptually, the wave stress driving the shorter waves is reduced from the total wind stress by progressively subtracting the wave stress associated with the longer waves. This approach allowed fine tuning the integrated wind input energy flux to closely balance the integrated energy loss rate due to breaking. This is an important validation check for the modeling, and we found that our sheltering algorithm provided wind stress estimates that agreed very closely with the observed levels as the wind sea aged. The modified Janssen (1991) wind input growth rate used in our calculations is also shown in Figure 1. Details about the wind input formulation are given in the Appendix.

3.3 Wind and wave model computations

We imposed a reference wind speed, U_{200}, at a height of 200m, and assumed a neutrally stable logarithmic atmospheric boundary layer structure over the sea.

$$U(z) = \frac{u_*}{\kappa} \log(\frac{z}{z_0})$$

To initialize and interrelate the boundary layer parameters, we also assumed the wave age dependent Charnock relation for the roughness length proposed by Donelan et al. (1993):

$$z_0 = 3.75e^{-5} (U_{10}^2 / g)(U_{10} / c_p)^{0.9}$$

The wind-wave model was initiated with a JONSWAP spectrum at a suitably short fetch, depending on the wind speed. Changes in the background wind field due to the waves impacted the wind stress that forced the wave model. This was subject to numerical control during the spin up period.

3.3.1 Computations of duration-limited wind wave evolution

Computations of the directional wave spectrum were made for the spectral bandwidth covering gravity waves from 0.01 Hz up to 5 Hz, using the source terms described above. We focused our development effort primarily on the case of a steady forcing wind speed of U_{10} = 12 m/s. This corresponded to the nominal wind speed conditions for the reported wave measurements during the FAIRS experiment, as seen in Figure 3(a) below.

Benchmark D (section 2.2.2) proved to be particular strategic significance. This involved a comparison of forecast and observed breaking wave properties during the growing seas of period 1, especially at the spectral peak where the proposed relationship (3) is most likely to be valid. This particular comparison has not been undertaken previously. Not only does this provide a tighter constraint on the form of the spectral dissipation rate source term, but it has the additional benefit of reducing the uncertainty in the form of S_{in}, as explained below.

We implemented and refined our modeling strategy for extracting the relevant wave breaking parameters, evaluating the wind stress components and coupling the wind and wave models so that a feedback was operative in which the computed wind stress forced the wave model interactively. Concurrently, we investigated breaking wave properties forecast at the spectral peak, validating the results using the newly available data from the FAIRS experiment on how

the spectral density of the breaker crest length changed as the wind sea aged (Gemmrich et al., 2008).

3.4 Extraction of breaking wave properties: Λ(c) and breaking strength b

The relationship (3) proposed by Phillips (1985) relates observed mean geometrical properties of whitecaps travelling with different speeds to the upper ocean spectral dissipation rate. Section 2.1.2 discussed the oversimplifications and shortcomings of (3), and section 3.2.1 describes how these have been addressed in this study. It is noted here that the form of (3) consistent with our spectral formulation is given by

$$S_{ds}^{loc}(c)\,dc = b\,g^{-2}c^{5}\Lambda(c)\,dc \qquad (5)$$

as the Phillips (1985) form for the spectral dissipation rate $\varepsilon(c) = g S_{ds}(c)$.

Banner and Morison (2008) provides the details of how the results of Banner et al. (2002) (section 2.1.1) and equation (4) can be used to find b and Λ from the numerical calculations of $S_{ds}(k)$ and normalized spectral saturation $\tilde{\sigma}$, evaluated at the spectral peak. The particular dependences in the Λ and S_{ds} spectra in these relations are appropriate to the computed or measured variables. The results are

$$\Lambda(c_p) = (\gamma g / 1.2\pi c_p^3) * Pr_{br}(\tilde{\sigma}_p) \qquad (6)$$

$$b_p = \frac{2.4\pi}{\gamma}\frac{g^2}{c_p^5}\frac{S_{ds}(k_p)}{Pr_{br}(\tilde{\sigma}_p)} \qquad (7)$$

with $Pr_{br}(\tilde{\sigma}_p) = H(\tilde{\sigma} - \tilde{\sigma}_T) * \alpha * (\tilde{\sigma} - \tilde{\sigma}_T)$, where $\tilde{\sigma}_T = 4.5\text{x}10^{-3}$ is the measured normalized spectral saturation breaking threshold, $\alpha \sim 33$, H is the Heaviside step function and $\gamma = 0.7$ for the spectral peak waves with the prescribed bandwidth $0.7 < c/c_p < 1.3$. The subscript p denotes the spectral peak.

These novel relations allow for the first time the breaking strength and crest length distributions of the dominant waves to be forecast from the output of a spectral wave model. However, there are potential sensitivities that need to be taken into account as they can affect the accuracy of the extracted breaking properties. They are associated with the rapid variation of the normalized spectral saturation $\tilde{\sigma}$ and local dissipation rate in the vicinity of the spectral peak, and the strong dependence of b on c_p.

4. RESULTS AND DISCUSSION

4.1 Breaking wave data analysis results

4.1.1 Breaking probabilities

The collaboration with Gemmrich and Farmer (IOS, Canada) analyzed the behaviour of breaking probability with scale using their 1999 Pacific Ocean storm waves data set. The directionally normalized spectral saturation $\tilde{\sigma}(f) = (2\pi)^4 f^5 F(f)/2g^2/\Theta(f)$, where f is the wave frequency, F(f) is the wave energy spectrum and $\Theta(f)$ is the directional spreading width spectrum. This study is described in detail in Banner et al. (2002).

The results shown below in Figure 2 reveal a remarkable near-uniform collapse for the breaking probability in different spectral bands at and above the spectral peak waves, and highlighted a common threshold of approximately 4.5×10^{-3} for breaking onset. These findings established order into the analysis of breaking wave measurements for the first time. In the present investigation, we used a formulation for S_{ds} for the dissipation rate associated with wave breaking that was based on this observed normalized saturation threshold. To this was added a term representing the dissipation rate due to background turbulence. This has been described in detail above in section 3.2.1.

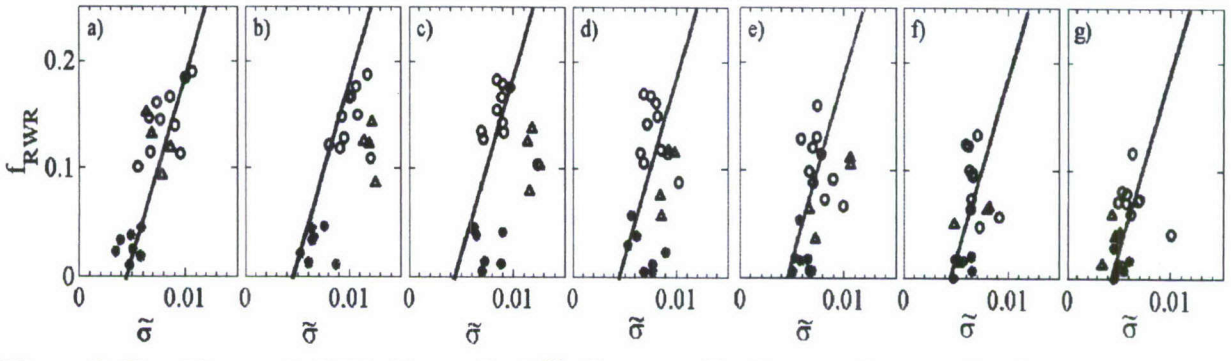

Figure 2. Breaking probability f_{rwr} against $\tilde{\sigma}$, the normalized spectral saturation for a range of spectral bands with center frequencies f_c/f_p (a) f_c/f_p=1.0 (b) f_c/f_p=1.16 (c) f_c/f_p=1.35 (d) f_c/f_p=1.57 (e) f_c/f_p=1.83 (f) f_c/f_p=2.13 (g) f_c/f_p=2.48. The symbols are one-hourly averages from three open ocean deployments where the wind speed exceeded 10 m/s.

4.1.2 Spectral density of breaking crest length/unit area

For reference in this report, the evolution of the sea state and meteorological conditions during the FAIRS experiment is shown in Figure 3(a), with results for the normalized wave saturation, suitably smoothed) shown in Figure 3(b). A unique feature of this data is seen in Figure 3(b) for the developing sea in period I. At the spectral peak, the normalized spectral saturation exceeds the breaking threshold, indicating breaking of the dominant waves. In periods II and III, the normalized spectral saturation for the spectral peak region is below the breaking threshold, and no breaking dominant waves are expected. The breaking wave phase speed histogram (Figure 4(a)) confirms this directly from a detailed video image analysis of the breakers. The breaker crest spectral density results from this analysis are shown in Figure 4(b), and this provides the key data for validating our numerical model, as described in detail below.

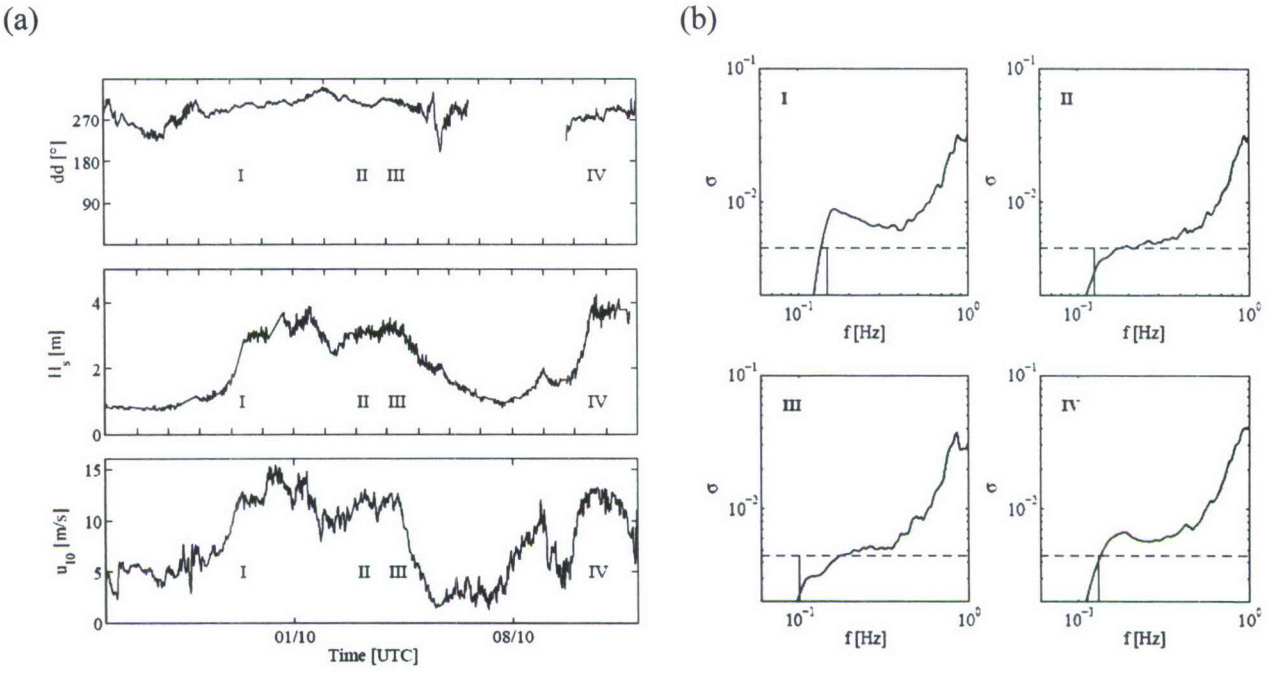

Figure 3. (a) Environmental conditions during the FAIRS experiment. Midpoints of individual data sets are marked I-IV. Top panel: wind direction dd; middle panel: significant wave height H_s; bottom panel: wind speed at 10m height u_{10} (b) Normalized wave saturation σ ($\tilde{\sigma}$ in text), (normalization is by the theoretical spreading distribution, as function of frequency f (data sets indicated in top left corner). Dashed horizontal line represents the common threshold for onset of breaking as determined in Banner et al. (2002). Vertical lines show the dominant wave frequency.

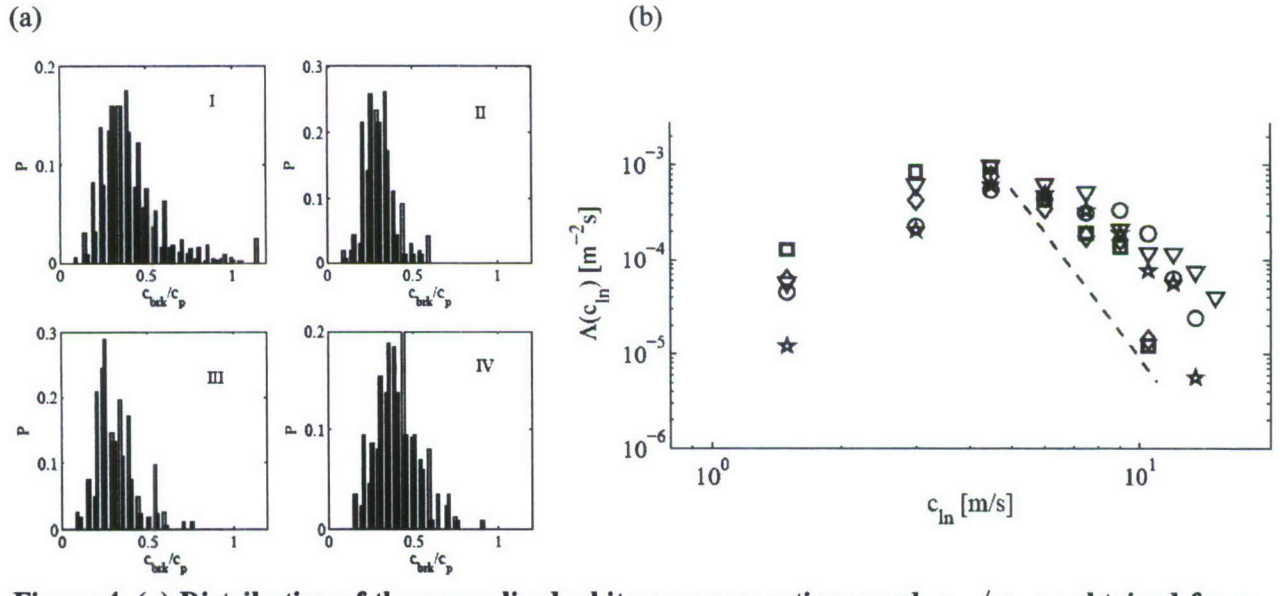

Figure 4. (a) Distribution of the normalized whitecap propagation speed c_{brk}/c_p as obtained from Camera 1 (gray bars) and Camera 2 (black bars). Individual panels correspond to the four data sets indicated in Figure 1. (b) Breaking crest length distribution $\Lambda(c_{br})$ as function of the breaker phase speed c_{br}. The symbols (○,▽,□,◇,⋆) correspond to data sets (Ia, Ib, II, III, IV), respectively. Ia and Ib are partititions of the data from period I where there were greater numbers of breakers. The dashed line shows the c^{-6} dependence, predicted by Phillips (1985).

4.2 Wave model evolution results

4.2.1 Standard wind speed U_{10}=12 m/s

We began by validating our model results for wave energy and spectral peak frequency against the duration-limited data trend curve given by Young (1999, §5.3.4) (benchmark A in section 2.2). It is seen in Figure 5 that our model closely reproduces these data trends. The modeled significant wave height (Figure 5(b)) closely matches the observed value of 3m for wave age 1.2.

(a)

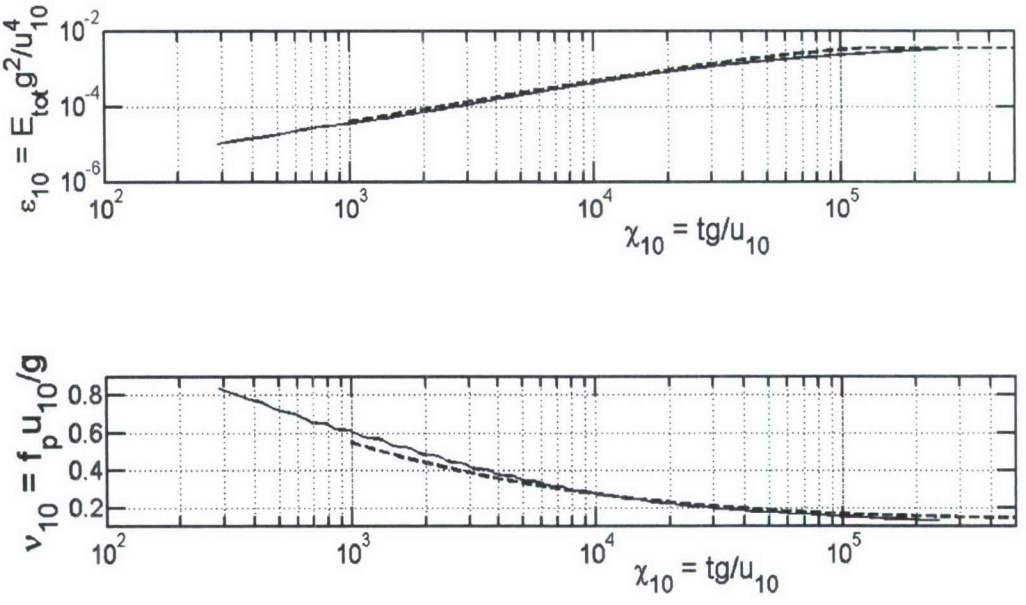

(b)

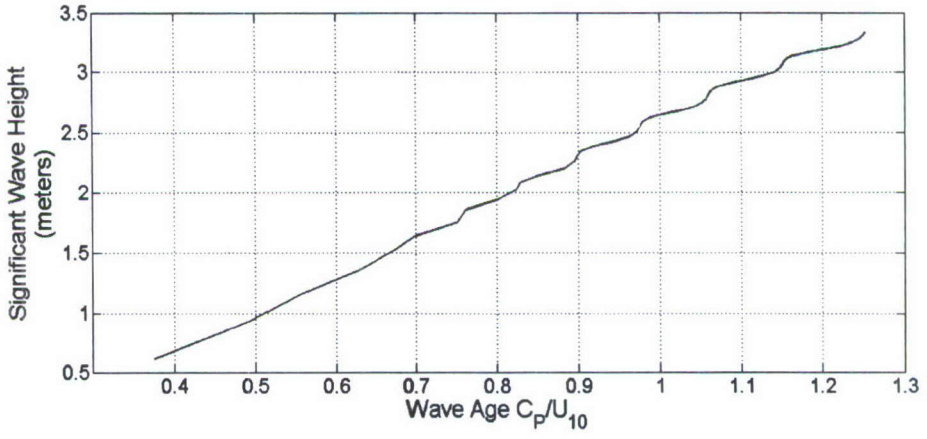

Figure 5. (a) Evolution of non-dimensional mean wave energy (upper panel) and spectral peak frequency (lower panel) against non-dimensional time for duration limited growth under U_{10}=12 m/s wind forcing. The background dashed lines are the trends of the data collated by Young (1999). (b) evolution of the significant wave height as the sea ages.

Benchmark B - spectral tail properties

The results for benchmark B in section 2.2 are shown in Figures 6 and 7. These spectral measures have been checked against available data and are in close agreement.

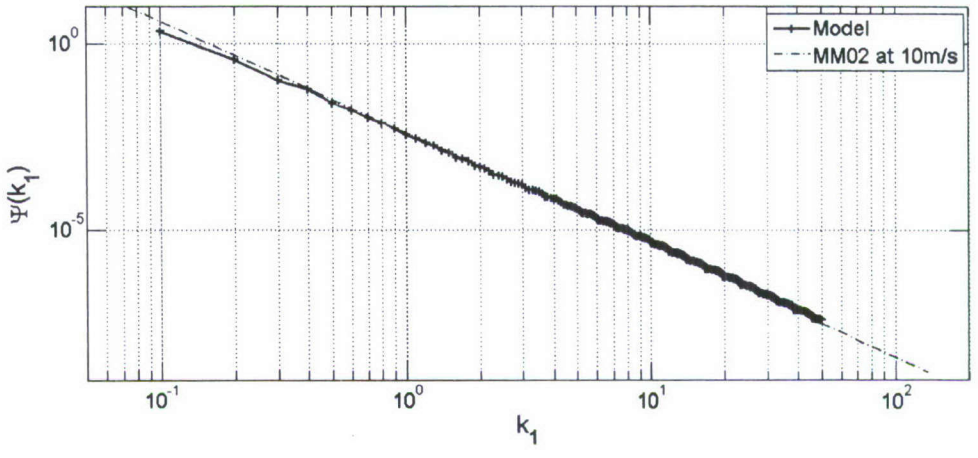

Figure 6. One-dimensional (k_1) wavenumber transect spectrum in the upwind-downwind direction, showing a close correspondence with the k_1^{-3} data trend of MM02 (Melville and Matusov, 2002), measured for very old wind seas in the U_{10} = 8-13 m/s range.

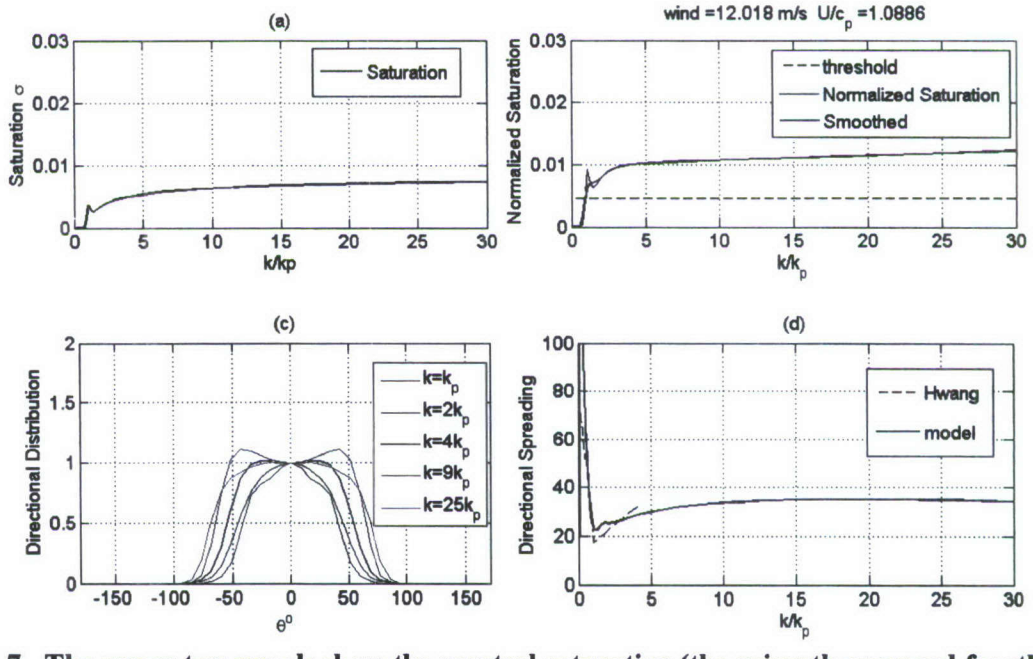

Figure 7. The upper two panels show the spectral saturation (the azimuth averaged fourth moment of the wavenumber spectrum). The left panel shows how the saturation changes with distance from the spectral peak. The right panel shows the corresponding behaviour of the saturation normalized by the corresponding mean directional spreading width. Also shown is the smoothed form using a 3 point area-preserving Poisson kernel. The directional spreading properties are seen in the lower two panels. The weakly bimodal angular spreading distributions at various distances from the spectral peak are seen in the left panel, while the right panel shows how the mean spreading width varies with distance from the spectral peak. The angle shown is the mean spreading half-width angle in degrees. The data in (d) is from Hwang *et al.* (2000) measured at a similar wave age.

Benchmark C - associated wind stress component and drag coefficient properties

Benchmark C is concerned with the relative size of wave-induced stress level in computational domain. The sum of the wave stress and the viscous tangential stress equals the total wind stress, which was measured in the FAIRS experiment.

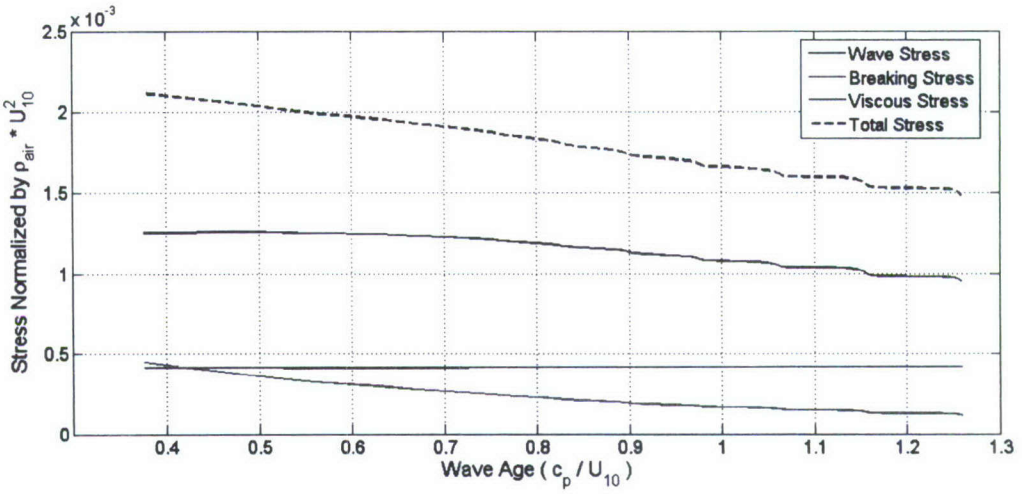

Figure 8. Behavior of the drag coefficient during the evolution from young to old wind sea conditions, showing the normalized wave stress, breaking wave stress and viscous tangential stress components. Descriptions of the individual stress terms are given in the Appendix.

The measured wind stress in FAIRS is equivalent to a drag coefficient of 1.7×10^{-3} for developing seas during period I (wave age ~ 0.92) and 1.45×10^{-3} for the mature wind seas (wave age ~ 1.22) during period III. The model results agree closely with these observed levels.

Benchmark D - breaking wave forecasts

A major goal of our model validation was to reproduce observed breaking statistics. The recent measurements of $\Lambda(c)$ reported by Gemmrich et al. (2008) shown in Fig. 4(b) are the most comprehensive and reliable observational database available. The spectral peak region results provide the most direct and basis for validation and our initial focus has been on this region. For the slower moving shorter breakers, the data shows the unexplained strong attenuation of Λ below c=3 m/s. This fall-off is consistent with previous measurements of distributional properties of breaking waves with decreasing speed (e.g. Li and Farmer, 2004).

Figure 9 shows modeled spectral distributions of $\Lambda(c)$ for wave ages corresponding to the periods I and III. These distributions were computed from equation (5) assuming a constant value of breaking strength $b=2 \times 10^{-5}$, which is the value reported by Gemmrich et al. (2008). This level was reproduced closely by our model results for the spectral peak breaking waves. The behaviour at the spectral peaks of the developing seas (period 1 where $c_{peak} \sim 11.0$ m/s) and mature seas (period 3 where $c_{peak} \sim 15.5$ m/s) are the primary focus of the comparison. The model predictions for the shorter waves are clearly not in accord with the data. This is discussed in detail below.

The results indicate very encouraging agreement between observed and forecast levels at the spectral peak during the developing sea state conditions. For 'fully-developed' seas, the model

produces no breaking at the spectral peak. Clearly, further comparisons with data are now needed to establish the robustness of the modeling approach proposed here.

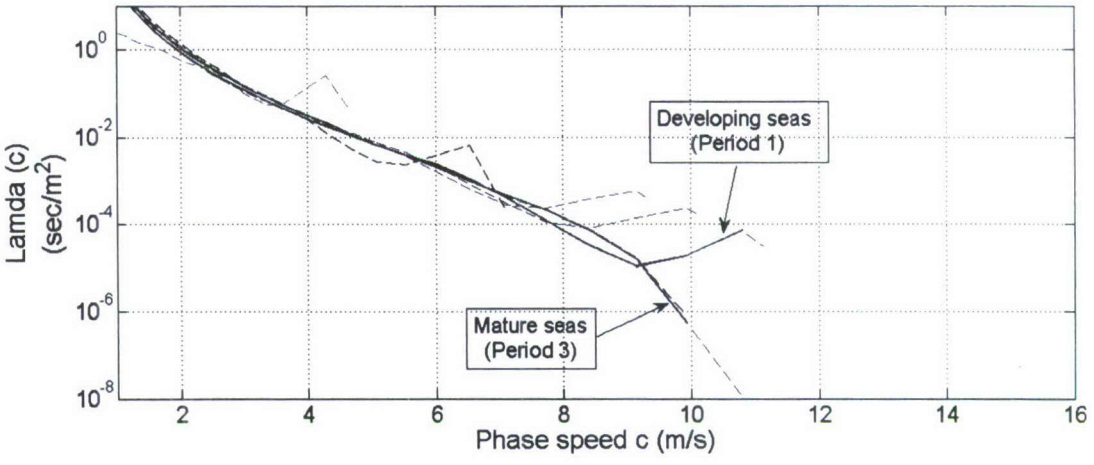

Figure 9. Model forecast of breaking wave crest length spectral density Λ(c) at different wave ages during the evolution for U_{10}=12 m/sec, assuming a constant value of breaking strength b=2x10^{-5}. Of particular interest are the red and black curves, corresponding to the sea state wave age conditions during periods I and III, where the spectral peak speeds were 11 m/sec and 15.5 m/sec respectively. Note that breaking at the spectral peak has ceased for the mature seas. The dashed curves for other (younger) wave ages are included for interest.

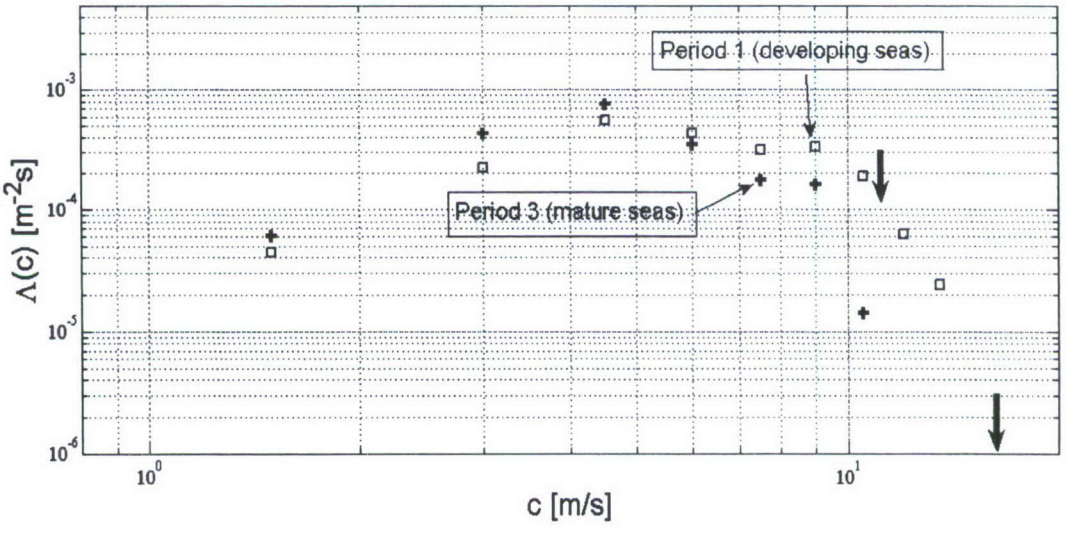

Figure 10. Measured breaking wave crest length spectral density Λ(c) for period I (blue circles and triangles) and period III (red circles) during the evolution for U_{10}=12 m/sec. The red and blue arrows indicate the spectral peaks corresponding to the wave age conditions during periods I and III, where the spectral peak speeds were 11 m/sec and 15.5 m/sec respectively.

For the slower moving shorter waves, it is evident that the model results depart substantially from the observations, with the former increasing while the latter maximizes and then decreases

towards slower wave speeds. The model behavior is constrained by equation (3), for which an alternate form with a nonlocal dependence could be envisaged. As mentioned above, observations show that the passage of breaking longer waves through shorter waves attenuates the short wave energy. This is additional to the short wave dissipation rate associated with the breaking of the short waves themselves. As this issue could not be resolved, it is left to be reconciled in the future. This limited our validation, and hence the present scope of our breaking wave forecasts, to the spectral subrange containing the fastest breaking waves, where these non-local dissipation issues are far less relevant. However, dissipation through background turbulence is still operative and is parameterized in S_{ds}, as described above in section 3.2.1 A.

A comparison of the observed and model results based on the assumed value for breaking strength $b=2x10^{-5}$ for the growing sea in Period I. The results for period I show a close correspondence between the observed and modeled spectral peak level of $\Lambda(c)$ of close to $1.0x10^{-4}$. For the mature sea state in Period III, the model predicts zero breaking at the spectral peak, as the normalized spectral saturation is below the threshold, also as seen in Figure 10(b). These conclusions are also confirmed in the observed breaking histograms shown in Figures 3 and 4.

The observed number of breakers during Period I of FAIRS in the adopted spectral peak bandwidth ($0.7<f/f_p<1.3$) is 41. The observed total crest count in the same bandwidth was measured as $0.7 * f_p^{-1}=353$, using our riding wave analysis code (Banner et al., 2002) on the FAIRS wave data. This gives a breaking probability of 0.062. For comparison, the modeled normalized spectral saturation gives $\tilde{\sigma} \doteq 0.0065$ at the spectral peak, for which the associate breaking probability $Pr_{br} = 0.066$, which corresponds closely to the observed breaking probability.

The observed $\Lambda(c_p)$ from Figure 10 for period I conditions ($U_{10}/c_p \sim 1.09$) is close to $1.0x10^{-4}$ sec/m^2. The associated value of $b=2.0x10^{-5}$ was reported by Gemmrich et al. (2008), and is a mean estimate across the whole spectrum of breaking waves.

Using our new methodology (equations (6) and (7)) for solving for both $\Lambda(c)$ and b for the spectral peak waves, $\Lambda(c_p) \sim 0.80x10^{-4}$ sec/m^2 and $b = 2.3x10^{-5}$. Given that it is the product $b\Lambda$ that determines the wave energy dissipation rate, it is evident that our new methodology provides results that are closely consistent with the FAIRS observational results reported by Gemmrich et al. (2008). While further field observational validation is required, the agreement of these initial results is very reassuring. To the extent possible, this phase of our effort met our modeling benchmark D.

Benchmark E - Overall consistency between wind input and dissipation rates

Driving the transition from growing to mature seas is the source term balance, shown below in Figure 11. A most interesting feature is that even though the wind input to the dominant waves decreases to well below the dissipation rate as the wave speed approaches the wind speed, the dominant wave saturation level (and steepness) remains sufficiently large for the breaking to occur through nonlinear wave group interactions (see Banner and Peirson (2007)).

Our proposed form (2) for S_{ds} is able to account for breaking onset and loss rates during the transition to swell. This situation arises for maturing wind seas, where the wind input to these longest waves has died away. The dominant waves are at the so-called Pierson-Moskowitz full development limit (e.g. see Alves et al., 2003). At this stage of evolution, the dominant balance

is between the dissipation and nonlinear transfer (see Figure 11b), where the dissipation is primarily background turbulence as the spectral peak saturation level is now below the breaking threshold. It is known that waves travelling faster than the wind input energy back to the airflow, and this reverse flux should be incorporated in the wind input source term as a negative contribution at the spectral peak. However, this was not needed for the present investigation and is left to future applications of this framework

(a)

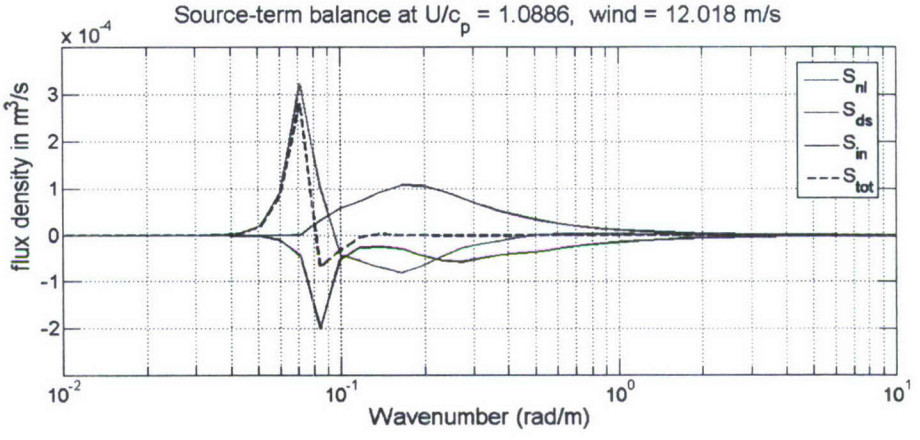

(b)

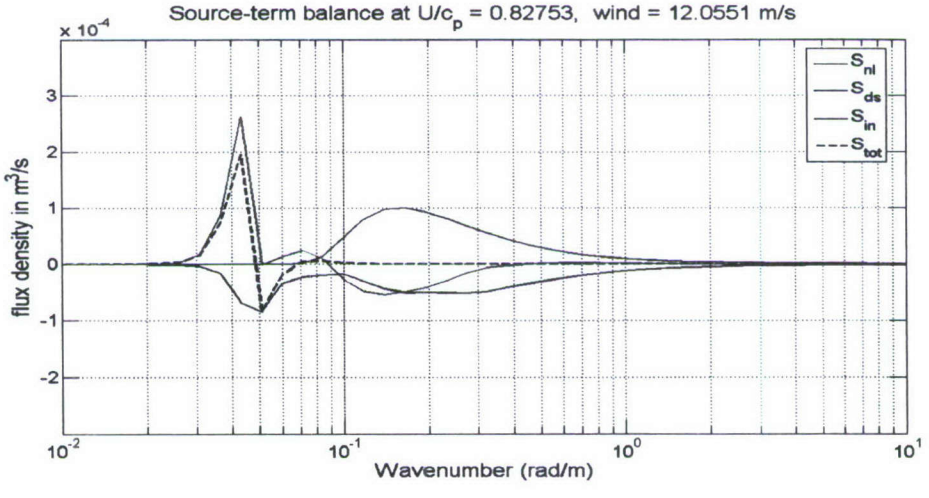

Figure 11. Source term balance for developing seas in period I (upper panel) and maturing seas period III (right panel). Note that even for period I, the dissipation rate at the spectral peak due to breaking is considerably larger than the wind input. For period III, there is negligible wind input and breaking at the spectral peak. The nonlinear transfer is reduced by the background dissipation. This is discussed in detail in the text above.

One further important validation check can be made on the closely related matter of total wave energy dissipation rate in the water column. During the FAIRS experiment, Gemmrich and Farmer (2004) made unique measurements of the dissipation rate just below the sea surface in the presence of the breaking waves. Using the Craig and Banner (1994) model to extrapolate

over the wave boundary layer and mixed layer, they estimated the total dissipation rate during period 2 was about 6.5×10^{-4} $m^3 sec^{-3}$. The corresponding level forecast for period I by our model is 5.3×10^{-4} $m^3 sec^{-3}$, decreasing to 4.2×10^{-4} $m^3 sec^{-3}$ for the mature seas in period III.

Given the numerous uncertainties in the parameters input to the Craig and Banner (1994) model, we also used the observational results of Fig. 6 in Terray et al. (1996) to estimate the total dissipation rate. For the evolving conditions of period I, $u_*^a / c_p \approx 0.048$, hence $\bar{c}/c_p \approx 0.23$, while for the mature period III waves, $u_*^a / c_p \approx 0.03$, hence $\bar{c}/c_p \approx 0.1$. The energy flux from the air to the water is then given by equation (5) in Terray et al. (1996):

$$F \approx \tau_a \, \bar{c} \, / \, \rho_{water} \, .$$

F closely approximates the turbulent energy flux from the breaking waves to turbulence in the water column. According to the Terray et al. (1996) data compilation, for the two observational periods I and III, the estimated integrated breaking wave energy fluxes (or total dissipation rates) are 5.3×10^{-4} $m^3 sec^{-3}$ and 2.2×10^{-4} $m^3 sec^{-3}$ respectively.

While our computed dissipation rates are marginally lower than the observational estimates, they are arguably within the observational uncertainty bounds. Given the intrinsic difficulty in making these measurements, we were very reassured by this aspect of the model validation. To the extent possible, benchmark E has been successfully addressed. The intrinsic value of this validation criterion motivates the future acquisition of further dissipation rate data, and indeed simultaneous wind input data, especially for higher wind speeds.

4.2.2 Model performance at severe wind speeds

The model diagnostics for U_{10}=12 m/s were very encouraging, so we carried out model runs at higher wind speeds of 18, 24, 36, 48 and 60 m/s to check the model performance for these more severe conditions ranging out to strong hurricane winds. It is important to note that the model settings were not modified for the higher wind speed cases explored. In the figures below, we show typical hurricane strength model performance for $U_{10} \sim 48$ m/s. The model performance at the other wind speeds was very similar. Thus benchmark A was fulfilled in terms of the evolution matching the standard growth curves very closely over the entire wind speed range we investigated (U_{10}= 6 to 60 m/s).

(a)

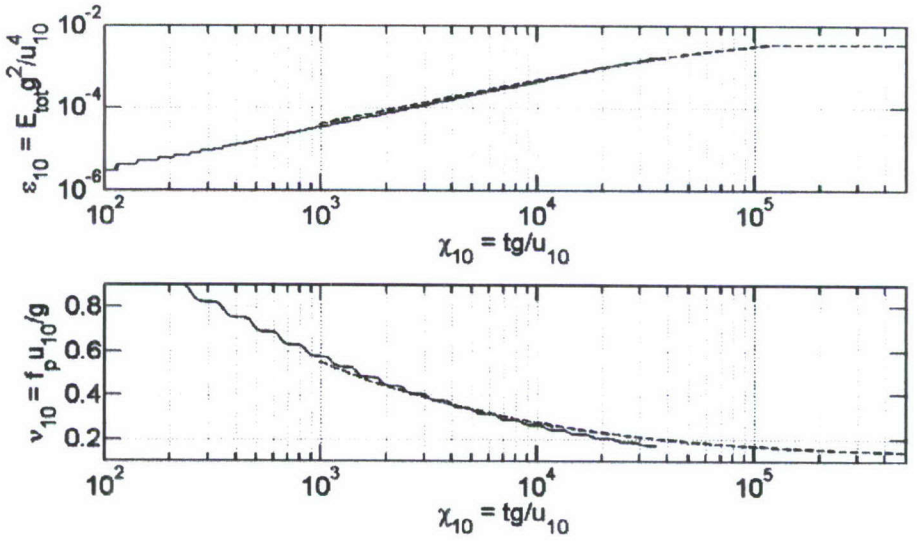

(b)

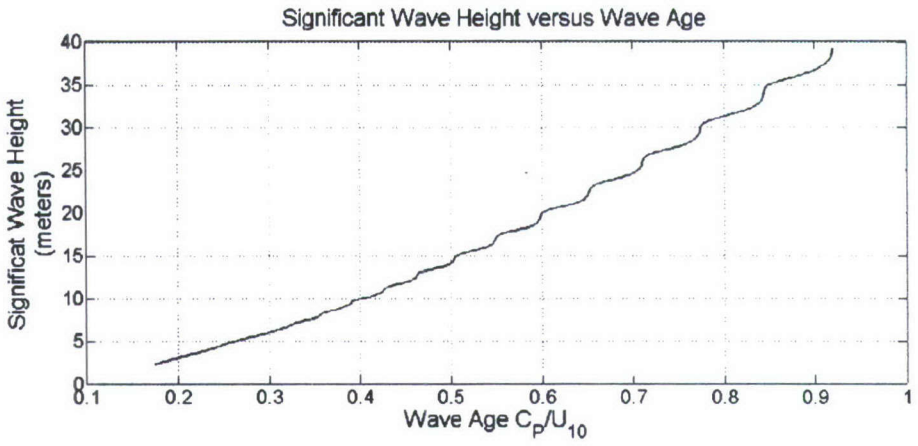

Figure 12 (a) evolution of the non-dimensional wave energy (upper panel) and non-dimensional dominant wave frequency (lower panel) against non-dimensional time for forcing by a hurricane wind speed U_{10} = 49 m/s. The background dashed curve is the trend of available field observations collated by Young (1999) (b) evolution of the significant wave height as the sea ages. Typical SWH for wave age 0.5 where the wind speed is twice the dominant wave speed is ~15 meters, and the corresponding wavelength is 370 meters. The jaggedness in the curves is a grid spacing artifice.

Benchmark B - predicted auxiliary properties of hurricane wave spectra

As with the standard 12 m/s wind speed case, each of the other wind speed cases showed very consistent and plausible spectral tail characteristics, consistent with observed behavior where such data is available. Examples from the nominal U_{10}~ 48m/s run at a wave age typical of hurricane conditions are seen in Figures 13 and 14 below. In Figure 13, the k^{-3} and weak wind speed dependence of the spectral level of the 1-D transect wavenumber spectrum are very encouraging, as they are consistent with data trends at much lower windspeeds.

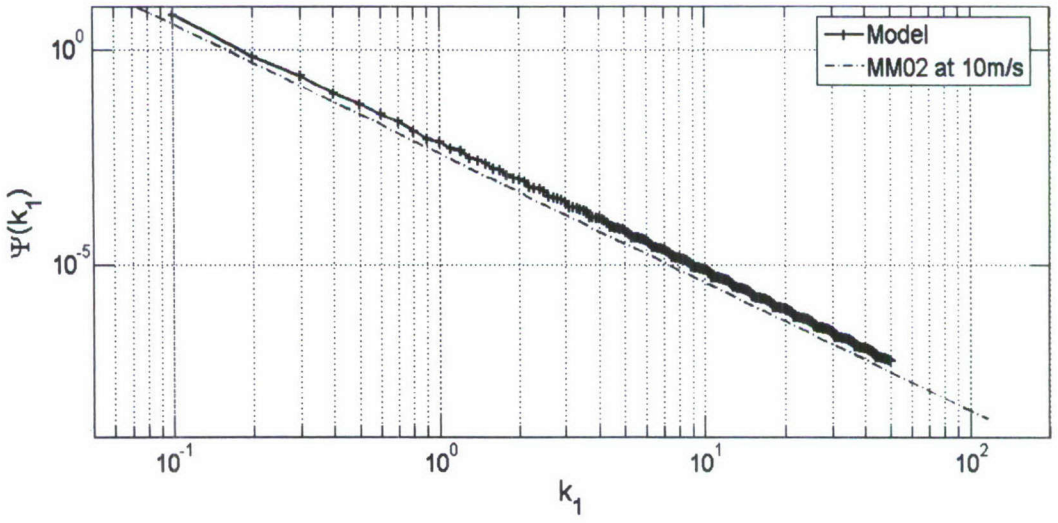

Figure 13. One-dimensional (k_1) transect wavenumber spectrum in the upwind-downwind direction for U_{10}=49 m/s and inverse wave age U_{10}/c_p~2. Note the close correspondence with the k_1^{-3} data trend of MM02 (Melville and Matusov, 2002), measured for old wind seas in the 8-13 m/s range.

In Figure 14, the angular spreading and spectral saturation characteristics conform to those at lower windspeeds. Based on the observed normalized spectral saturation, the predicted dominant breaking probability for this case is 0.21. Direct observational validation of this potentially observable statistic would be very valuable.

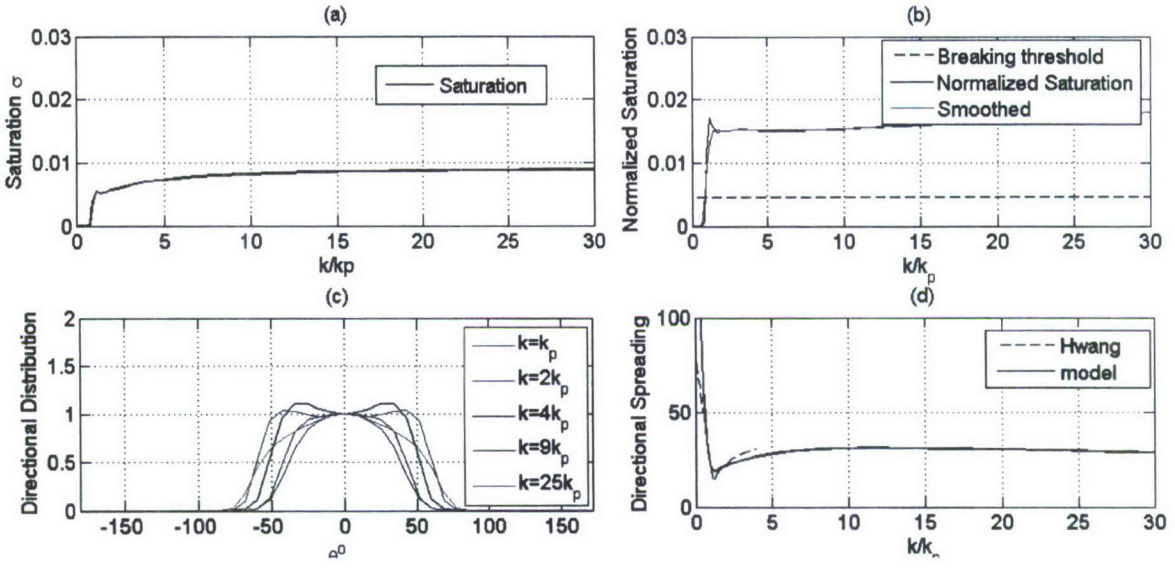

Figure 14. Spectral properties for hurricane wind speed (49 m/s) and inverse wave age U_{10}/c_p~2. The dominant wavelength is close to 370m. The upper two panels show the spectral saturation (the azimuth averaged fourth moment of the wavenumber spectrum). The left panel shows how the saturation changes with distance from the spectral peak. The right panel shows the corresponding behaviour of the saturation normalized by the corresponding mean directional spreading width. Also shown is the smoothed form using a 3 point area-preserving Poisson kernel. The directional spreading properties are seen in the lower two panels. The weakly bimodal angular spreading distributions at various distances from the spectral peak are seen in the left panel, while the right panel shows how the mean spreading width varies with distance from the spectral peak. The angle shown is the mean spreading half-width angle in degrees. The data in (d) is from Hwang et al. (2000) measured at a similar wave age, but for U_{10}=9.5 m/s.

Benchmark C - associated wind stress component and drag coefficient properties

Figure 15 below shows the behavior of the drag coefficient during the evolution from young to old wind sea conditions, with the individual contributions arising from the wave-induced wind stress, additional breaking wave wind stress and viscous tangential stress components. Descriptions of these individual stress terms are given in the Appendix. Noteworthy is the relatively low value of the total drag coefficient, which is well below the extrapolated linear trend of measured drag coefficients at moderate wind speeds below U_{10}~20 m/s. Despite the sparse data available and its intrinsically large scatter, the modeled drag coefficient levels are consistent with the observed trend for which the drag coefficient tends to level off or even decrease as the wind speeds approach severe-to-hurricane strength (e.g. see Fig. 5 in Black et al., 2007).

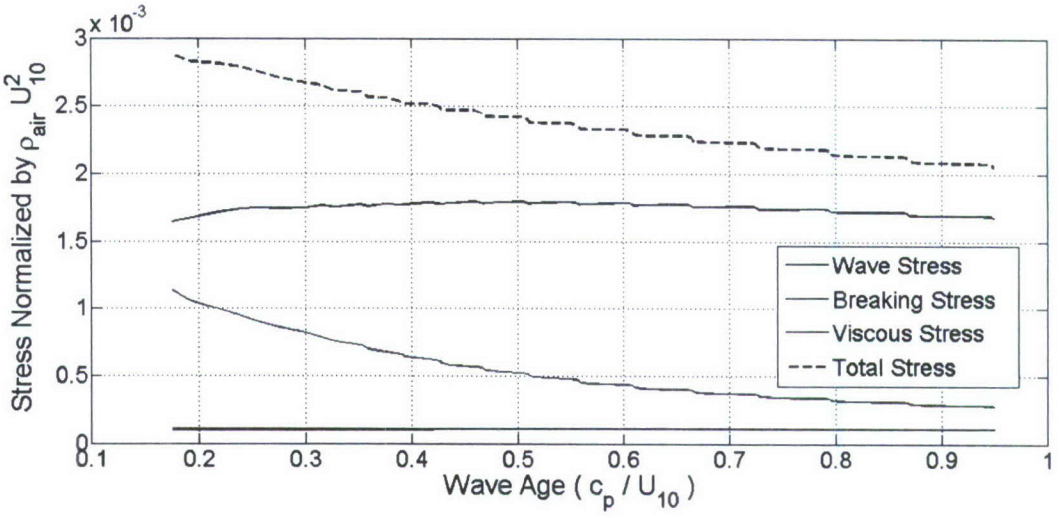

Figure 15. Behavior of the drag coefficient during the evolution from young to old wind sea conditions, showing the normalized wave stress, breaking wave stress and viscous tangential stress components. Descriptions of the individual stress terms are given in the Appendix. Note the low value of the drag coefficient, which is consistent with its observed attenuation for hurricane winds.

Benchmark D - associated breaking wave properties

The absence of measured breaking wave data and associated wind wave spectra in hurricane conditions precludes making a direct validation of the breaking dominant wave properties at this time. It was anticipated that the whitecap data gathered synchronously with SRA data during the CBLAST flights would be very useful for this purpose, but this data was not published by the time this report was compiled and hence validation against observations must await the future availability of this data.

Breaking predictions for 48 m/s windspeed

For a typical young wind sea with $U_{10}/c_p \sim 2$, with $U_{10} \sim 48$ m/s, using the model results in equations (6) and (7) predicts $\Lambda(c_p)=2.8\text{x}10^{-5}$ sec/m^2 with a corresponding breaking strength $b=1.6\text{x}10^{-4}$.

In comparison, a similar calculation for 12 m/s winds for the same inverse wave age $U_{10}/c_p \sim 2$ predicts $\Lambda(c_p)= 2.6\text{x}10^{-3}$ sec/m^2 and a corresponding breaking strength $b=6.0\text{x}10^{-5}$. These results indicate that for a fourfold wind speed increase, the breaking crest length spectral density decreases by a factor of about 100 while the breaking strength decreases by a factor of only 2. Taking into account the 4 times larger magnitude of the spectral peak bandwidth at the higher wind speed, the actual change in the mean spectral peak breaking crest length is about 25 times higher at the lower wind speed.

These calculations indicate that as the wind sea ages for a given wind speed, both the breaking crest length spectral density and the corresponding local breaking strength decrease. A systematic analysis of the predicted breaking properties of the dominant waves over a wide range of wind speeds and sea states will be given in Morison and Banner (2008).

Benchmark E - Overall consistency between wind input and dissipation rates

We verified that during the evolution at each wind speed, the integrated wind input and dissipation rates closely tracked each other, with the dissipation rate approaching the wind input

rate as the seas age. The integrated nonlinear transfer term was zero at each timestep. Given that the total wind input to the waves is less than the total wind input to the sea surface, and that the drag coefficients were realistic, it is believed that the modelled dissipation rates are also very plausible.

4.2.3 Summary of model results

In this study, a framework for incorporating wave breaking predictions of breaking crest length density and strength of the dominant wind waves into sea state forecast models has been developed. It has been validated under the assumption that it will be implemented in conjunction with the exact form of the nonlinear spectral transfer term S_{nl}, together with a suitable wind input source term formulation S_{in}. Because of the computational cost, our validations have been limited to idealized cases, particularly duration-limited, uni-directional (but possibly non-stationary) winds. These cases provided a cost-effective but limited validation regime and further validation is needed, especially of breaking wave data for severe wind speeds.

The model framework developed has performed very well over a particularly wide range of wind speeds according to the five benchmarks designed to provide a critical testbed of the model's capabilities. The outcome is that the model is in principle ready for implementation into an operational prototype, as recommended in 4.4 below.

4.3 Full coupling of the wave model to the wind field

With the very encouraging validation to date of our 'semi-coupled' framework, it is feasible to transition it to a fully coupled version. This would require a full atmospheric model, using a suitable wind input growth rate parameterization that ideally would depend on a scale-dependent wind velocity, such as $U(\lambda/2)$, where λ is the water wavelength. This is left as a future extension.

4.4 Transition to operations

The breaking wave model framework developed in this project has been built around the 'Exact' NL source term for S_{nl}, as we sought to choose the most accurate source terms, albeit at the cost of computational speed. However, the approximate form of S_{nl} in widespread operational use, known as the Direct Interaction Approximation (DIA), at each timestep computes only one of the wave-wave resonance interaction terms of the millions that are computed by the 'Exact' NL source term. Needless to say, the results can be very different, and we wanted to eliminate this from our model development.

A much closer approximation known as the Two-Scale Approximation (TSA) has been developed recently (Resio and Perry, 2008). Its performance appears to match the Exact NL very closely and hence may be a suitable replacement for Exact NL in operations. This is an exciting and timely development that needs careful examination.

4.5 Highlights of the SPANDEX study

SPANDEX, the Spray Production and Dynamics Experiment, is a laboratory study conducted at the UNSW Water Research Laboratory in Manly Vale, Sydney, Australia. The goals of SPANDEX were to illuminate physical aspects of spume droplet production and dispersion, verify theoretical simplifications presently used to estimate the source function from ambient droplet concentration measurements, and examine the relationship between the implied source strength and forcing parameters such as wind speed, surface turbulent stress, and wave properties. Our observations of droplet profiles give reasonable confirmation of the basic power-

law profile relationship that is commonly used to relate droplet concentrations to the surface source strength. This essentially confirms that, even in a wind tunnel, there is a near balance between droplet production and removal by gravitational settling. Phase Doppler Anemometry observations revealed significant mean horizontal and vertical slip velocities that were larger closer to the surface. The magnitude seems too large to be an acceleration time scale effect, so we hypothesize that the droplets tend to be found in vertically moving air masses (e.g., updrafts departing from wave crests). Scaling of the droplet production surface source strength proved to be difficult to explain quantitatively. The wind speed forcing varied only 23% and the stress increased by a factor of 2.2. Yet, the source strength increased by about a factor of 10. We attempted to relate this to an estimate of surface wave energy flux through calculation of the standard deviation of small-scale surface disturbance combined with wind forcing. This energy flux index only increased 52% with the wind forcing, so it is not clear that we have characterized energy flux correctly. Nonetheless, a graph of spray mass surface flux versus surface disturbance energy is quasi-linear with a substantial threshold.

4.6 Benefits Analysis Summary

4.6.1 Technical Output

This project has produced several refereed publications in leading journals, as well as conference and workshop contributions.

Refereed papers published

Banner, M.L., J.R. Gemmrich & D.M. Farmer, 2002: Multiscale measurements of ocean wave breaking probability. *J. Phys. Oceanogr.* 32, 3364-3375.

Banner, M.L. & W.L. Peirson, 2007: Wave breaking onset and strength for two-dimensional deep water wave groups. *J. Fluid Mech.*, 585, 93-115.

Gemmrich, J.R., M.L. Banner & C. Garrett, 2008: Spectrally resolved energy dissipation and momentum flux of breaking waves. *J. Phys. Oceanogr.* 38, 1296-1312.

Refereed papers submitted

Fairall, C.W., M.L. Banner, W.L. Peirson, W. Asher & R.P. Morison, 2008: Investigation of the physical scaling of sea spray spume droplet production. Submitted to *J. Geophys. Res. (Oceans)*, May, 2008.

Refereed papers to be submitted

The following two manuscripts are in an advanced stage of preparation and will be submitted to *Ocean Modeling* by the end of 2008.

Banner, M.L. & R.P. Morison, 2008: Forecasting wave breaking in ocean wind wave models. Part I. Model framework and validation against field data.

R.P. Morison & M.L. Banner, 2008: Forecasting wave breaking in ocean wind wave models. Part II. Model performance for severe wind forcing.

Conference papers published

Forecasting Breaking Waves during Storms, Michael L. Banner, Ekaterini Kriezi and Russel P. Morison, 2004: Proc. 8th International Workshop On Wave Hindcasting and Forecasting, Honolulu, Hawaii, September 24-29, 2004

On Modeling Spectral Dissipation due to Wave Breaking for Ocean Wind Waves, 2006: Michael L. Banner[1] and Russel P. Morison. Proc. 9th International Workshop On Wave Hindcasting and Forecasting, Victoria, B.C., Canada, September 24-29, 2006

Recent Progress on Understanding and Modelling Ocean Wave Breaking, 2007: M.L. Banner, W.L. Peirson and R.P. Morison. In 'New Trends in Fluid Mechanics Research', Proc. Fifth International Conf. on Fluid Mechanics, Aug. 15-19, Shanghai, Tsinghua U. Press & Springer.

Research seminars presented

University of Miami, RSMAS: 12/2003 Recent Progress On Ocean Wave Breaking

CBLAST Hurricane Workshop, RSMAS, 02/ 2004: Recent Progress on Breaking Wave Modeling & Sea Spray Physics

Swinburne University, 09/2004 Forecasting Breaking Waves During Storms

Seattle APS Meeting 11/2004 Forecasting Breaking Waves During Storms

Sydney University 10/2004 Forecasting Breaking Waves During Storms

WISE Workshop ECMWF, Reading, UK 06/2004 Modeling Wave Breaking in Spectral Wind Wave Models – a Current Perspective

Australian Meteorological and Oceanographic Society International Conference on Storms, Brisbane, 07/2004: Towards Improved Sea State Forecasts During Storms

CBLAST Hurricane Workshop, RSMAS, 04/2005: Recent Progress on Breaking Wave Prediction & Enhancements to Air-Sea Fluxes

WISE Workshop Toronto Canada 06/2005 On Modeling Wave Breaking In Spectral Wind Wave Models – The Latest Challenges

AGU Ocean Sciences, Honolulu, 10/2006: Recent Progress on Forecasting Breaking Waves

WISE Workshop, 04/2007: On Modeling Spectral Dissipation Due to Wave Breaking for Ocean Wind Waves

4.6.2 Strategic Implications

Negotiations are underway with Dr. H. Tolman, Head, Modeling Branch, NOAA to investigate transitioning this modeling framework for forecasting breaking of the dominant sea waves into WaveWatch III. We are also discussing possible participation in a forthcoming NOPP wave modeling source term review proposal.

Acknowledgements

The authors gratefully acknowledge the support from ONR during the course of this study. The effort of Johannes Gemmrich in analyzing the FAIRS field data was pivotal to the progress of this project. We also benefited from technical discussions with our former colleague Tony Elfouhaily who is greatly missed, and interactions with CBLAST colleagues Ed Walsh and Pete Black on CBLAST hurricane wave and whitecap data.

References

Alves, J.H and M.L. Banner, 2003: Performance of a saturation-based dissipation source term for wind wave spectral modelling, *J. Phys. Oceanogr.* 33, 1274-1298.

Banner, M.L., I.S.F Jones and J.C.Trinder, 1989: Wavenumber spectra of short gravity waves. *J. Fluid Mech.* 198, 321-344.

Banner, M.L., 1990a: The influence of wave breaking on the surface pressure distribution in wind wave interactions. *J. Fluid Mech.* 211, 465-493.

Banner, M.L., J.R. Gemmrich and D.M. Farmer, 2002: Multiscale measurements of ocean wave breaking probability. *J. Phys. Oceanogr.* 32, 3364-3375.

Banner, M.L. and W.L. Peirson, 1998: Tangential stress beneath wind-driven air-water interfaces. *J. Fluid Mech.* 364, 115-145.

Banner, M.L. & Peregrine, D.H., 1993: Wave breaking in deep water. *Ann. Rev. Fluid Mech.,* 25, 373-397

M.L. Banner & W.L. Peirson, 2007: Wave breaking onset and strength for two-dimensional deep water wave groups. *J. Fluid Mech.*, 585, 93-115.

Black, P.G., E.A. D'Asaro, W.D. Drennan, J.R. French, P.P. Niiler, T.B. Sanford, E.J. Terrill and E.J. Walsh, 2007: Air_sea exchange in hurricanes. Synthesis of observations from the Coupled Boundary Layer Air-Sea Transfer Experiment. BAMS March 2007, AMS, 357-374. DOI:10.1175/BAMS-88-3-357.

Donelan, M.A., F.W. Dobson, S.D. Smith & R.J. Anderson, 1993: On the Dependence of Sea Surface Roughness on Wave Development, *J. Phys. Oceanogr*, 23, 2143-2149.

Donelan, M.A., A.V. Babanin, I.R.Young and M.L. Banner, 2006: Wave follower field measurements of the wind input spectral function. Part II. Parameterization of the wind input. J. Phys. Oceanogr., 36, 1672-1688.

Gemmrich, J. R. & Farmer, D.M., 2004: Near-surface turbulence in the presence of breaking waves. *J. Phys. Oceanogr*, 34, 1067-1086.

Gemmrich, J.R., M.L. Banner, M.L. & C. Garrett, 2008: Spectrally resolved energy dissipation and momentum flux of breaking waves. *J. Phys. Oceanogr*. In press.

Hsiao, S.V., and O.H. Shemdin, 1983: Measurements of wind velocity and pressure with a wave follower during MARSEN. *J. Geophys. Res.*, 88, 9841-9849.

Hwang, P.A., D.W. Wang, E.J. Walsh, W.B. Krabill & R.W. Swift, 2000: Airborne measurements of the wavenumber spectra of ocean surface waves. Part II: Directional distribution. *J. Phys. Oceanogr.*, 30, 2768-2787.

Hwang, P.A. and D.W. Wang, 2004: Field measurements of duration-limited growth of wind-generated ocean surface waves at young stage of development. *J. Phys. Oceanogr.*, 34, 2316-2326.

Janssen, P.A.E.M., 1991: Quasi-linear theory of wind-wave generation applied to wave forecasting. *J. Phys. Oceanogr.*, 21, 1631-1642.

Komen, G.J., L. Cavaleri, M.A. Donelan, K. Hasselmann, S. Hasselmann & P.A.E.M. Janssen, 1994: Dynamics and Modelling of Ocean Waves, Cambridge University Press, Cambridge, 532pp.

Makin, V.K. and V.N. Kudryavtsev, 2001: Coupled sea surface-atmosphere model. 1. Wind over waves coupling. *J. Geophys. Res.* 104, 7613-7623.

Melville, W.K. and P. Matusov, 2002: Distribution of breaking waves at the ocean surface. *Nature*, 417, 58-63.

Melville, W.K., 1996: The role of surface-wave breaking in air-sea interaction. *Ann. Rev. Fluid Mech*, **26**, 279-321

Miles, J.W., 1957: On the generation of surface waves by shear flows. *J. Fluid Mech.* 3, 185-204.

Phillips, O.M., 1985: Spectral and statistical properties of the equilibrium range in wind-generated gravity waves. *J. Fluid Mech.*, 156, 505-531.

Plant, W.J., 1982: A relation between wind stress and wave slope. *J. Geophys. Res.* 87, 1961-1967.

Song, J. & M. L. Banner, 2002: On determining the onset and strength of breaking for deep water waves. Part 1: Unforced irrotational wave groups. *J. Phys. Oceanogr.* **32**, 2541-2558.

Snyder, R.L, F.W. Dobson, J.A. Elliott, and R.B. Long, 1981 : Array measurements of atmospheric pressure fluctuations above surface gravity waves. *J. Fluid Mech.* 102, 1-59.

Terray, E.A., M.A. Donelan, Y.C. Agrawal, W.M. Drennan, K.K. Kahma, A.J. Williams III, P.A. Hwang, and S.A. Kitaigorodskii, 1996: Estimates of kinetic energy dissipation under breaking waves. *J. Phys. Oceanogr.*, 26, 792-807

Tian, Z, M. Perlin & W. Choi, 2008: Evaluation of a deep-water breaking criterion. *Phys. Fluids* 20, 066604. DOI: 10.1063/1.2939396

Thorpe, S.A., 1993: Energy loss by breaking waves. *J. Phys. Oceanogr.*, 23, 2498-2502

Tracy, B.A. and D.T. Resio, 1982: Theory and calculation of the nonlinear energy transfer between se waves in deep water, WIS Rept 11, US Army Engineers Waterway Experiment Station.

Young, I.R., 1999: Wind generated ocean waves. Elsevier, 288 pp.

Appendix: Details of the wind input source term

We implemented a modified form of the Janssen (1991) wind input growth rate formulation, with a 'sheltering' term designed to reduce the growth rates to the slower moving, shorter wave components. This was done to maintain the overall aerodynamic drag coefficient at levels consistent with observed levels.

Sheltering strategy

The total aerodynamic drag is the sum of the wave drag, the breaking wave drag and the tangential stress, i.e. $\tau_{tot} = \tau_w + \tau_{bw} + \tau_{tang}$

The wave stress is expressed as $\tau_w = \gamma \Phi(k,\theta)/c$, where the growth rate γ is given below.

The breaking wave stress is expressed as $\tau_{bw}(\mathbf{k}) = Pr_{br}(\mathbf{k}) * Fr(\mathbf{k}) * \tau_w(\mathbf{k})$. Here, $Pr_{br}(\mathbf{k})$ is the breaking probability at scale **k** and Fr(**k**) is the ratio of actual crests to Fourier modes at scale **k**. For details on how $Pr_{br}(\mathbf{k})$ and Fr(**k**) are defined and parameterized based on observations, see Banner et al (2000).

The tangential stress parameterization is expressed as $\tau_{tang}=$

This was based on the on the tangential drag coefficient behaviour reported by Banner and Peirson (1998). They observed that the tangential drag coefficient was a decreasing function of the wind speed, largely independent of the wave age. We developed a parameterization that conformed to their data trend at moderate wind speeds, and asymptoted to a residual level of 0.0001 for hurricane winds of 50 m/s. This is based on the assumption that no matter how strong and widespread the air flow separation becomes, the wind always maintains some residual re-attachment to the water surface, where the tangential stress will be non-zero.

In the present modeling, the overall friction velocity is given by $u_* = \sqrt{\tau_{tot}}$. Also, a reduced friction velocity felt by the n^{th} wavenumber k_n, which reflects the sheltering of the short waves by the longer waves, is given by

$$u_*^{red}(k_n) = \sqrt{\tau_{tot} - \sum_{i=1}^{n} (\tau_w(i) + \tau_{bw}(i))} \qquad \text{for } 1 \le n \le N$$

where N is the total number of wavenumber grid points. At each timestep, the model recalculates the total and local u_* levels, which are then fed back into the wind input source term. This key aspect of the wind input source term is described in the following section.

Modified Janssen (1991) wind input growth rate formulation

Following Janssen (1991), define $\mu = (u_*/\kappa c)^2 (g z_0 / u_*^2) \exp(J_1 \kappa / (u_* \cos\theta / c)^2)$ where $\kappa = 0.4$ is the Karman constant, $J_1 = 0.99$, c is the phase speed and θ is the direction of the waves relative to the wind.

The Miles parameter is given by $\beta = J_2 \mu (\ln(\mu))^4 / \kappa^2$, for $\mu \le 1$ and $\beta = 0$ for $\mu > 1$, where $J_2 = 1.6$.

The spectral growth rate is then given by $\gamma(k,\theta) = \varepsilon\beta\omega\,(u_*^{red}(k)\cos\theta/c)^2$, where ε is the ratio of air to water densities, and the corresponding wind input source term is $\gamma E(k,\theta)$. Note that the form of the Janssen (1991) growth rate parameterization has been largely followed, with the Miles coupling parameter based on the overall u_*/c but we have modified the input to the shorter waves by using u_*^{red} in the quadratic forcing term.

Figure 1 in section 3.2.1 of this report indicates the extent of the sheltering modification to Janssen (1991) for representative young (wave age=0.5) wind sea conditions, when the wave field is growing strongly under wind forcing. This reduction in wind input to the spectral tail is maintained as the wind sea ages.